

AUG 4 1981

Item 830-H-15

NAS 1.60:1831

NASA Technical Paper 1331

COMPLETED

ORIGINAL

Analytical Prediction and Experimental  
Verification of Performance, at  
Various Operating Conditions,  
of a Dual-Mode Traveling Wave Tube  
With Multistage Depressed Collectors

James A. Dayton, Jr., Henry G. Kosmahl,  
Peter Ramins, and Norbert Stankiewicz

JULY 1981

**NASA**

NASA Technical Paper 1831

Analytical Prediction and Experimental  
Verification of Performance, at  
Various Operating Conditions,  
of a Dual-Mode Traveling Wave Tube  
With Multistage Depressed Collectors

James A. Dayton, Jr., Henry G. Kosmahl,  
Peter Ramins, and Norbert Stankiewicz  
*Lewis Research Center*  
*Cleveland, Ohio*



National Aeronautics  
and Space Administration

**Scientific and Technical  
Information Branch**

1981

Blank Page

## Summary

A computational design procedure is described for traveling wave tubes (TWT's) that use spent beam refocusing and multistage depressed collectors (MDC's) for efficiency enhancement. Experimental and analytical results are compared for a high performance, octave bandwidth, dual-mode TWT operated over a wide range of conditions. The computations were carried out with advanced computer programs that model the electron beam as a series of either disks or rings of charge and follow their multidimensional trajectories from the radiofrequency (rf) input of the ideal TWT through the slow wave structure and the magnetic refocusing system to their points of impact in the depressed collector. TWT performance, collector efficiency, and collector current distribution were computed, and the results were compared with measurements for a number of TWT-MDC systems. Power conservation and correct accounting of TWT and collector losses were observed.

In general, very good agreement was obtained between computed and measured collector efficiencies, and the computer design of a highly efficient MDC was demonstrated. The analytical tools used herein appear to be sufficiently refined to design efficient collectors for this class of TWT. For maximum efficiency, some experimental optimization (e.g., collector voltages and aperture sizes) will most likely be required. For TWT's of higher perveance and electronic efficiency, additional verification of the design process is needed.

## Introduction

In a joint USAF-NASA program, the Lewis Research Center is carrying out an experimental and analytical program to improve the efficiency of traveling wave tubes (TWT's) for use in electronic countermeasure systems by applying multistage depressed collector (MDC) (refs. 1 and 2) and spent beam refocusing (refs. 3 and 4) techniques originally developed at Lewis for amplifiers for communication satellites.

The analytical phase of this work involves two computer programs that follow the electron beam from the input of the TWT to its impact in the MDC.

The first is a highly accurate program that carries out the large signal analysis of the performance of broadband TWT's. This computer program also describes the characteristics of the spent electron beam emerging from the TWT with sufficient accuracy to be used as input data for the second computer program that is used in the design and analysis of the spent beam refocusing systems and MDC's. Applying these two programs can minimize the number of experimental design iterations needed to meet a set of performance requirements, thus significantly reducing the development time and cost of new designs.

An experimental program stresses accurate and complete TWT-MDC performance evaluations. Because complete measurements are made in terms of electron flow and power conservation, it is possible to compare in considerable detail the analytically predicted and experimentally determined TWT and MDC performances. The experimental configuration illustrated in figure 1 shows the electron gun, helix slow wave circuit, refocusing coils, and MDC.

In references 5 and 6 the computer models were described in detail, and comparisons of analytical predictions and experimental measurements for a number of TWT-MDC systems were presented. In general, very good agreement was found between computed and measured MDC efficiencies.

In a continuation of this program, the work has been extended to cover the operation of a dual-mode

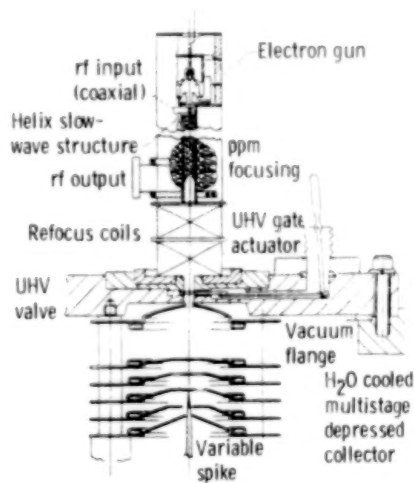


Figure 1. - Experimental configuration.

TWT and MDC over a wide range of conditions to simulate the applications where—

(1) the TWT is pulsed at saturation between the low and high modes;

(2) a large (10:1) pulse-up capability in output power is needed, and low mode represents TWT operation well below saturation;

(3) the TWT must be operated at constant output power in the linear low distortion range.

In this paper, the results of the TWT, refocusing system, and MDC analyses are discussed, and a comparison is made of the analytical and experimental results obtained for the various TWT operating conditions. In addition, the computer programs were used to design a small, highly efficient collector for use with this TWT. This design and a comparison of the analytically predicted results with the experimental results at the design operating conditions are presented herein. A detailed presentation of the optimized experimental results over a wide range in operating conditions is presented in reference 7.

## Analytical Models and Computer Programs

### TWT-Refocuser-MDC-System

The analytical model illustrated in figure 2 presents a detailed picture of electron current and power flow in the TWT-refocuser-MDC system. For purposes of analysis, the TWT with an MDC is divided into four parts:

- (1) The TWT between the radiofrequency (rf) input and rf output
- (2) A drift region past the rf output in a continuation of the focusing magnetic field
- (3) The refocusing region
- (4) The MDC

The electron beam is modeled as a series of 32 deformable disks (or alternatively 96 rings) of charge per rf cycle, and the trajectories of the disks are tracked (successively) through each of these regions with proper matchup at the interfaces. The Lewis Research Center's large-signal, multidimensional, helical TWT program was used for TWT and drift region analysis (refs. 5 and 6). A version of the Stanford Linear Accelerator Center (SLAC) computer program developed by Herrmannsfeldt (ref. 8) was used for the refocuser and MDC analysis.

### Traveling Wave Tube

In the TWT, disk trajectories in the presence of rf circuit forces, space charge forces, and magnetic

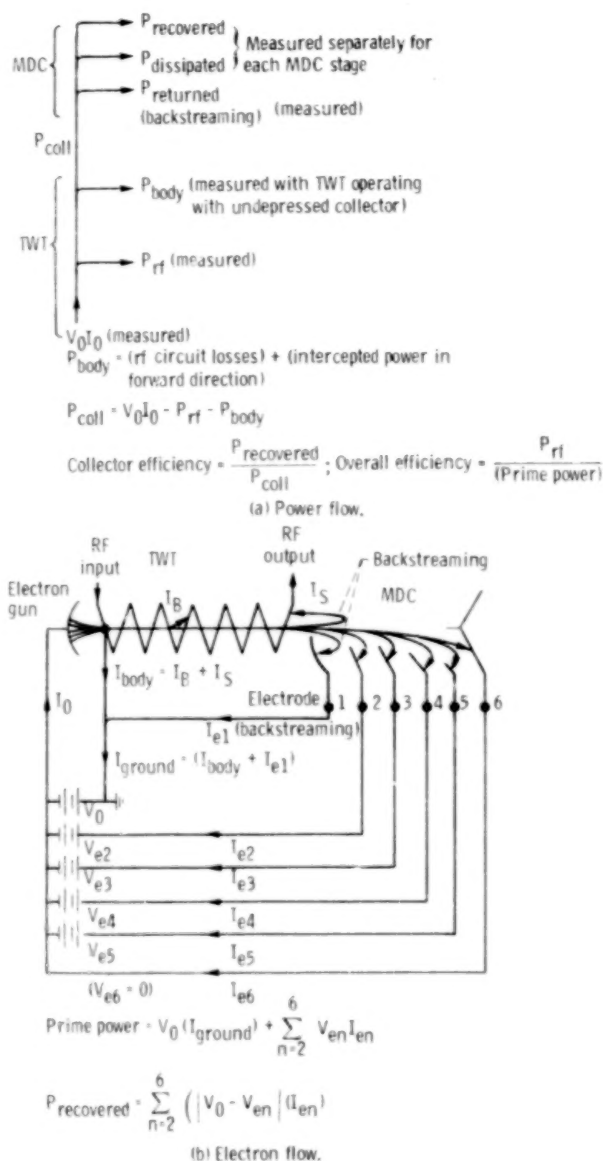


Figure 2. - Flow diagrams for TWT with five-stage depressed collector.

focusing fields are computed from the rf input of the TWT to the rf output.

At the rf output the computer program lists the following:

- (1) rf output power
- (2) rf circuit losses
- (3) Severe and attenuator losses
- (4) Intercepted current and power
- (5) Radial coordinates of the disk edges
- (6) Three components of velocity ( $\dot{r}, \dot{\phi}, \dot{z}$ ) of each disk
- (7) Relative phase of each disk

The trajectory program does not include effects of thermal velocities on the radial and azimuthal motion. According to Herrmann's optical theory of



thermal electrons, these effects are negligible for medium and high space charge ( $\mu_{perv} > 0.5$ ) and substantial for small space charge ( $\mu_{perv} < 0.1$ ).

### Drift Region

At the rf output the beam is tightly bunched and strong space charge forces can exist between the disks. As the beam drifts beyond the rf output while remaining confined by the focusing magnetic field, the resulting energy exchange between disks can lead to a significantly altered spent beam energy distribution that, in turn, could significantly alter an optimum MDC design (ref. 6). This debunching is analyzed by continuing the disk trajectory calculation beyond the rf output in a continuation of magnetic focusing but with no rf circuit forces present. The beam characteristics (disk position coordinates and vector velocities) at the end of this drift region define the input conditions to the refocusing system.

### Refocuser

In the refocusing calculation, the basic assumption is made that axial debunching has occurred in the rf field free region before the beam is injected into the refocuser as discussed previously. If debunching had not occurred, it would be necessary to solve a dynamic, time-dependent problem rather than the steady-state problem that is assumed. Each disk of charge in the TWT model is replaced in the refocusing section and MDC by a continuous ray of current. This current ray is located at the centroid of charge of the disk and has the vector velocity of the disk centroid. Current ray trajectories in the presence of the magnetic refocusing fields and space charge are computed through the refocuser. The beam characteristics (current ray position coordinates and vector velocities) at the end of the refocusing define the input conditions to the MDC.

### Multistage Depressed Collector

In the MDC analysis, the trajectory calculation is continued until the current rays impact on the MDC electrodes. In the real collector, secondary electron emission occurs when electrons impact on the electrode surfaces. The effects of secondary electron emission can only be estimated. It is assumed herein that all charge impacts on the MDC electrodes generate only low-energy secondaries with the local electric field determining whether they are suppressed or accelerated to less depressed electrodes. In these calculations a yield of 0.4 secondary electrons per primary electron was used since a coating of carbon

black was used on the experimental collector electrodes.

Based on the entrance conditions and the position of final collection of each ray, the following are computed: current to each of the electrodes, backstreaming current and power to the TWT (if any), power recovered by each of the electrodes, and kinetic power dissipated on each of the electrodes. These results when coupled with the outputs of the TWT computer program provide a detailed picture of the current and power flow within the TWT-MDC system.

## Experimental Program

The experimental program was designed to measure the various powers, currents, and voltages shown in the power flow and electron flow diagrams (fig. 2), permitting a detailed comparison with the analytical results. The experimental techniques are described in detail in reference 9.

## TWT Characteristics

A modified version of the Teledyne MEC dual-mode TWT model MTZ-7000 (serial number 103) was used in this program. The modification included the additions of—

- (1) a short drift section past the rf output in a continuation of the magnetic focusing;
- (2) a Lewis designed variable spent beam refocusing system;
- (3) Lewis designed five- and four-stage depressed collectors.

The general TWT characteristics are as follows:

Operating frequency, GHz.....	4.8 to 9.6
Beam voltage, kV .....	9.9
Beam current, A.....	
High mode .....	0.49
Low mode .....	0.38
Maximum output power, W.....	
High mode .....	830
Low mode .....	530

The tube is focused with periodic permanent magnets (PPM).

## Analytical and Experimental Procedure

The TWT-MDC performance was both analyzed and experimentally evaluated at six distinct operating conditions at 8.4 gigahertz. The analysis employed the 32-disk model and the cosine formulation of

PPM focusing as described in reference 5. These operating conditions were selected to simulate the following TWT applications:

(1) The TWT is pulsed at saturation between the low and high modes.

(2) The TWT is pulsed between the low and high modes, but the low mode represents operation well below saturation.

(3) The TWT is operated in the low mode at constant output power in the linear low distortion range at two representative levels of electronic efficiency.

The TWT analysis was first performed for the high mode at saturation using the TWT parameters supplied by the manufacturer. The analysis was performed for the TWT type rather than for the individual model tested: TWT's of identical design do not have identical operating parameters or performance. The TWT performance in the low mode (at and below saturation) was then obtained by adjusting only the beam current and rf input power. The experimental program was conducted concurrently with the TWT analysis using an existing refocusing system and MDC added to the TWT (ref. 9). The refocusing system profile and MDC operating conditions were experimentally optimized for each of the applications discussed previously. For the first two applications a compromise optimization was involved since the refocusing field profile and MDC operating conditions had to remain fixed as the TWT was pulsed between various operating conditions. Therefore, less than optimum performance resulted in one or both modes. The magnetic fields used in the refocusing computation were ideal coil representations (refs. 10 and 11) of these optimized profiles ( $B_z(r=0,z)$  vs.  $z$ ). The precise MDC voltages and geometries were used in the MDC computation.

The next sections give the results of the TWT, refocusing system, and MDC analyses and a detailed comparison of analytical and experimental performance in terms of the electron and power flows in the TWT-MDC system.

## Results of Helical TWT Program

### Dual-Mode Operation at Saturation

The spent beam energy distributions for the high and low modes at saturation are shown in figures 3(a) and (b), respectively. The range of electron energies is larger for the high mode because of the larger beam perveance and electronic efficiency (ref. 12).

The spent beam continues through an extension of PPM focusing ( $1\frac{1}{4}$  magnetic periods) where, with the rf forces removed, debunching and some beam

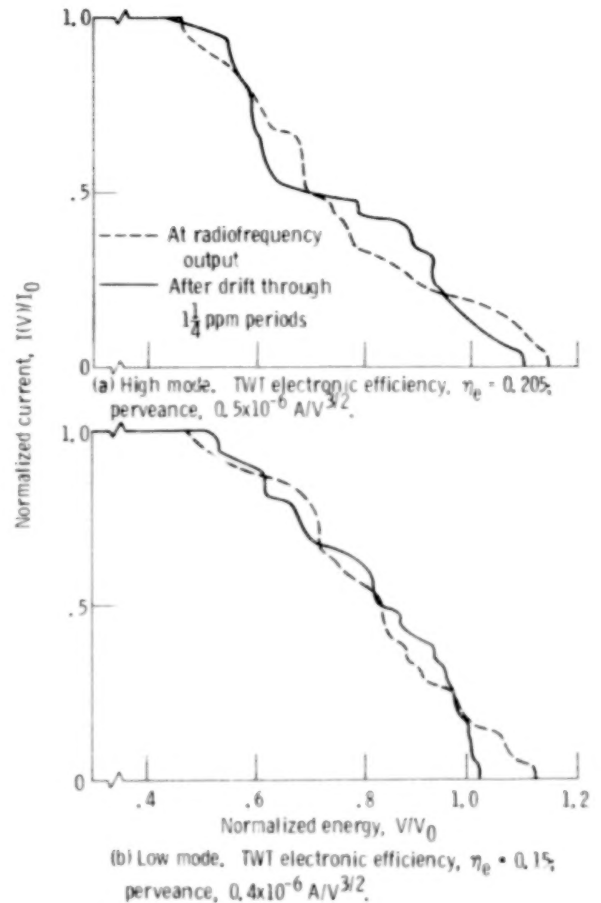


Figure 3. - Computed spent beam energy distribution before and after debunching for TWT operation at saturation.

expansion occur. The resulting energy distributions after debunching are also shown in figures 3(a) and (b) for the high and low modes, respectively. Comparing the results before and after debunching shows that, for both modes, the effect was sufficient to change appreciably the optimum set of MDC voltages. In general, the effect is beneficial: the slow electrons speed up and the fast ones slow down.

The spent beam energy distributions for the high and low modes at the input to the refocusing system are compared in figure 4. It is clear that even without consideration of beam size and electron angles optimum MDC's for each of the modes would be somewhat different. Therefore, a compromise is involved in the MDC design for dual-mode operation.

### Dual-Mode TWT Operation Over a 10:1 Pulse-Up in Output Power

The computed spent beam energy distributions after debunching for the operation of the dual-mode TWT over a 10:1 range in output powers are shown

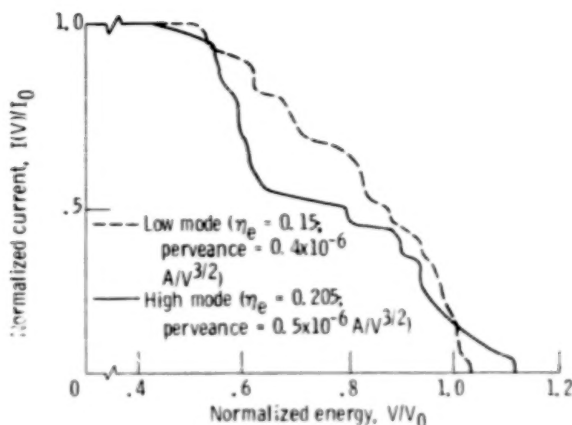


Figure 4. - Computed spent beam energy distributions of high and low modes at saturation after debunching.

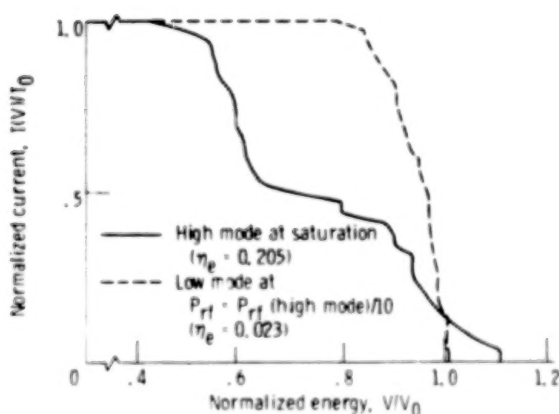


Figure 5. - Computed spent beam energy distributions for operation of dual-mode TWT over 10:1 range in radio-frequency powers (after debunching).

in figure 5. The two beams differ greatly in character, and optimum MDC's for each of these modes would be quite different. Therefore, a considerable compromise is involved in the MDC design, and substantially less than the optimum efficiencies can be expected for one or both of the modes.

### TWT Operation in the Linear Range

The computed spent beam energy distributions for operation in the linear range (electronic efficiency of 4 and 2 percent) are compared with the saturated low mode case in figure 6. For operation increasingly below saturation the range of electron energies narrows and increasingly higher collector efficiencies can be expected (ref. 12).

At the end of the drift region only a small amount of beam expansion has taken place and many electrons are moving inward toward the axis (the

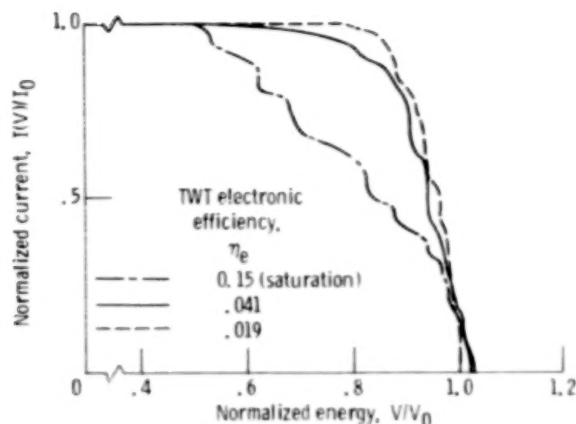


Figure 6. - Computed spent beam energy distributions at and below saturation (low mode after debunching).

negative angles in tables I to III). These difficulties are remedied by the refocusing system.

## Refocusing Analysis Results

### Dual-Mode TWT Operation at Saturation

The charge trajectories through the refocusing region for the high and low modes are shown in figures 7(a) and (b), respectively. The input angles to and output angles from the refocusing system are shown in tables I(a) and (b) for the high and low modes, respectively.

Beam (area) expansion is by factors of 18 and 11 for the high and low modes, respectively. During this expansion, most of the energy that is associated with rotational kinetic energy and space charge potential (depression) is converted to recoverable axial kinetic energy, an additional benefit of spent beam refocusing.

The refocusing field profile ( $B_z(r=0, z)$  vs.  $z$ ) is shown in figure 7. This profile was experimentally optimized for the low mode and, starting with the chaotic beam at the input, produced the well ordered, nearly parallel beam at the refocusing system output (fig. 7(b)). For the high mode, however, the beam is slightly overfocused (the negative output angles of table I(a) and fig. 7(a)) and of larger diameter at the input to the collector.

### Dual-Mode TWT Operation Over a 10:1 Pulse-Up in Output Power

The charge trajectories through the refocusing region for the high and low modes are shown in figures 8(a) and (b), respectively. The input angles to and output angles from the refocusing system are shown in tables II(a) and (b).



TABLE I. - INPUT AND OUTPUT ANGLES OF REFOCUSING  
SYSTEM FOR SATURATED OPERATION

(a) High mode			(b) Low mode		
Trajectory	Input angle, <sup>a</sup> deg	Output angle, <sup>b</sup> deg	Trajectory	Input angle deg	Output angle, <sup>b</sup> deg
1	-5.0	-0.8	1	-3.5	1.7
2	3.6	-3.8	2	-2.7	-.1
3	-5.8	1.8	3	2.8	-1.0
4	-3.5	1.6	4	3.4	-1.2
5	3.9	-2.1	5	-2.3	1.0
6	-2.8	1.4	6	0	.2
7	-1.0	1.9	7	-2.5	1.7
8	2.3	-3.2	8	-3.2	1.1
9	-3.2	1.2	9	-4.5	1.8
10	.4	.5	10	-3.4	.7
11	.7	-1.4	11	-2.8	1.0
12	.7	.7	12	-.7	1.7
13	2.8	-.6	13	.9	.6
14	3.3	-1.1	14	0	.3
15	.9	-1.3	15	-2.8	1.0
16	-2.8	1.2	16	-2.5	1.2
17	3.3	-.8	17	-.5	2.0
18	0	1.5	18	1.4	.7
19	-4.8	.4	19	-3.3	.2
20	-3.6	.5	20	-.3	1.4
21	1.4	.2	21	-.6	1.6
22	-.3	1.7	22	-2.8	.5
23	1.5	2.0	23	-1.8	1.2
24	-4.3	3.1	24	.2	1.6
25	.2	1.9	25	2.7	2.2
26	.7	1.9	26	2.1	1.4
27	-3.0	.3	27	3.2	1.3
28	.7	1.5	28	-4.2	3.4
29	-.6	.8	29	-.5	1.8
30	-2.6	.5	30	.1	1.8
31	-1.1	.9	31	-1.9	1.8
32	-.5	1.5	32	1.8	2.5

<sup>a</sup>For centroid of charge; average radius,  $\bar{r}$ , 0.046 cm.

<sup>b</sup>For centroid of charge; average radius,  $\bar{r}$ , 0.193 cm.

<sup>a</sup>For centroid of charge; average radius,  $\bar{r}$ , 0.051 cm.

<sup>b</sup>For centroid of charge; average radius,  $\bar{r}$ , 0.165 cm.

TABLE II. - INPUT AND OUTPUT ANGLES OF REFOCUSING  
SYSTEM FOR 10:1 PULSE-UP IN OUTPUT POWER

(a) High mode

Trajectory	Input angle, <sup>a</sup> deg	Output angle, <sup>b</sup> deg
1	-0.7	4.1
2	-2.3	2.5
3	-1.6	2.9
4	.3	4.3
5	.3	4.2
6	-1.8	2.9
7	.3	4.2
8	.9	4.4
9	-.3	3.9
10	.6	3.9
11	-.2	3.0
12	-.7	3.5
13	-1.5	.2
14	-.4	2.5
15	.7	3.7
16	-.6	3.5
17	1.5	4.4
18	-.7	.8
19	.3	3.4
20	-.5	1.9
21	-1.9	.9
22	-.9	.7
23	-.6	1.3
24	1.0	3.8
25	-.3	1.8
26	-.7	1.8
27	-.6	1.4
28	-.5	3.3
29	-.5	1.9
30	-.1	2.7
31	.2	2.6
32	.3	2.9

(b) Low mode

Trajectory	Input angle, <sup>a</sup> deg	Output angle, <sup>b</sup> deg
1	-5.0	4.3
2	3.6	2.4
3	-5.8	2.8
4	-3.5	2.4
5	3.9	3.4
6	-2.8	3.3
7	-1.0	3.3
8	2.3	2.2
9	-3.2	3.0
10	.4	4.1
11	.7	3.1
12	.7	4.1
13	2.8	3.9
14	3.3	3.7
15	.9	3.1
16	-2.8	2.9
17	-3.3	3.8
18	0	3.9
19	-4.8	1.0
20	-3.6	1.5
21	1.4	3.1
22	-.3	3.5
23	1.5	4.2
24	-4.3	4.7
24	.2	2.6
26	.7	3.9
27	-3.0	1.3
28	.7	3.8
29	-.6	2.8
30	-2.6	.7
31	-1.1	2.4
32	-.5	2.9

<sup>a</sup>For centroid of charge; average radius,  $\bar{r}$ , 0.051 cm.

<sup>b</sup>For centroid of charge; average radius,  $\bar{r}$ , 0.27 cm.

<sup>a</sup>For centroid of charge; average radius,  $\bar{r}$ , 0.046 cm.

<sup>b</sup>For centroid of charge; average radius,  $\bar{r}$ , 0.19 cm.

TABLE III. - INPUT AND OUTPUT ANGLES OF REFOCUSING  
SYSTEM FOR OPERATION OF TWT IN LINEAR RANGE

(a) TWT electronic efficiency,  
 $\eta_e$ , 0.04

Trajectory	Input angle, <sup>a</sup> deg	Output angle, <sup>b</sup> deg
1	-2.3	3.5
2	-1.7	2.6
3	-3.7	2.4
4	.5	2.7
5	-2.8	2.4
6	-.8	2.8
7	-2.3	2.3
8	.4	2.4
9	-1.6	2.2
10	.9	3.1
11	-1.9	2.4
12	-2.8	1.4
13	.6	2.9
14	-1.1	2.6
15	-.5	2.8
16	.3	2.9
17	-3.0	1.8
18	.3	2.6
19	.3	3.0
20	-.8	2.6
21	.5	3.0
22	-.1	2.8
23	-.1	2.5
24	-2.3	.9
25	.2	2.9
26	.4	2.9
27	-1.5	2.0
28	-1.4	2.2
29	-1.0	2.4
30	-2.5	1.3
31	-1.2	2.1
32	-1.9	1.7

(b) TWT electronic efficiency,  
 $\eta_e$ , 0.02

Trajectory	Input angle, <sup>a</sup> deg	Output angle, <sup>b</sup> deg
1	-0.6	3.3
2	-2.6	1.3
3	.2	3.7
4	-.3	3.5
5	-2.3	.8
6	-1.3	3.1
7	.3	3.2
8	.2	3.3
9	-1.8	1.0
10	1.0	2.9
11	-1.1	2.6
12	-.3	3.2
13	-.3	2.7
14	-.7	3.2
15	-2.1	1.9
16	-1.8	1.8
17	1.3	3.8
18	.6	3.2
19	.5	3.3
20	.2	2.6
21	-.1	3.2
22	-.9	2.4
23	.2	3.3
24	-1.0	2.0
25	-.5	1.1
26	-.9	1.5
27	.4	3.0
28	.3	3.2
29	-.5	2.3
30	-.5	2.6
31	-1.2	.8
32	-1.5	.9

<sup>a</sup>For centroid of charge; average radius,  $\bar{r}$ , 0.048 cm.

<sup>b</sup>For centroid of charge; average radius,  $\bar{r}$ , 0.163 cm.

<sup>a</sup>For centroid of charge; average radius,  $\bar{r}$ , 0.047 cm.

<sup>b</sup>For centroid of charge; average radius,  $\bar{r}$ , 0.17 cm.

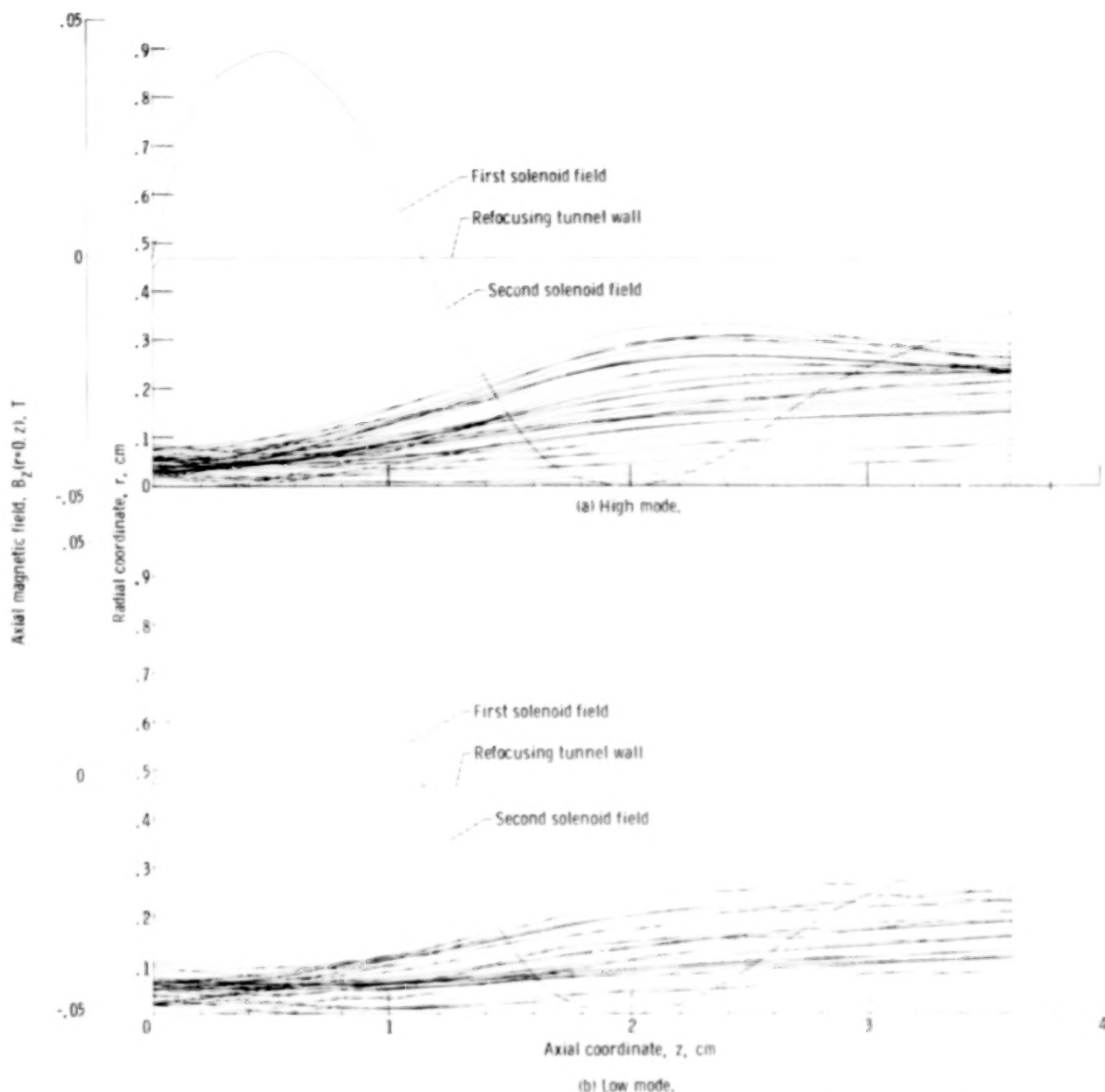


Figure 7. - Charge trajectories and refocusing field profile in refocusing section for TWT operation at saturation.

The refocusing field profile, shown in figure 8, was optimized largely for the low mode and produced the well ordered beam with all the charges having positive angles, shown in figure 8(b).

For the high mode, however, the beam expansion is excessive, almost resulting in interception on the tunnel walls. Also, some angles are larger than desired.

#### TWT Operation in the Linear Range

The charge trajectories through the refocusing

region for operation of the TWT at electronic efficiencies of 4 and 2 percent are shown in figures 9(a) and (b), respectively. The input angles to and output angles from the refocusing system are shown in tables III(a) and (b).

The refocusing system profiles, shown in figures 9(a) and (b), were individually optimized for each case. These optimum profiles produced the well ordered beams, shown in figures 9(a) and (b), with all the charges having small positive angles at the input to the MDC.

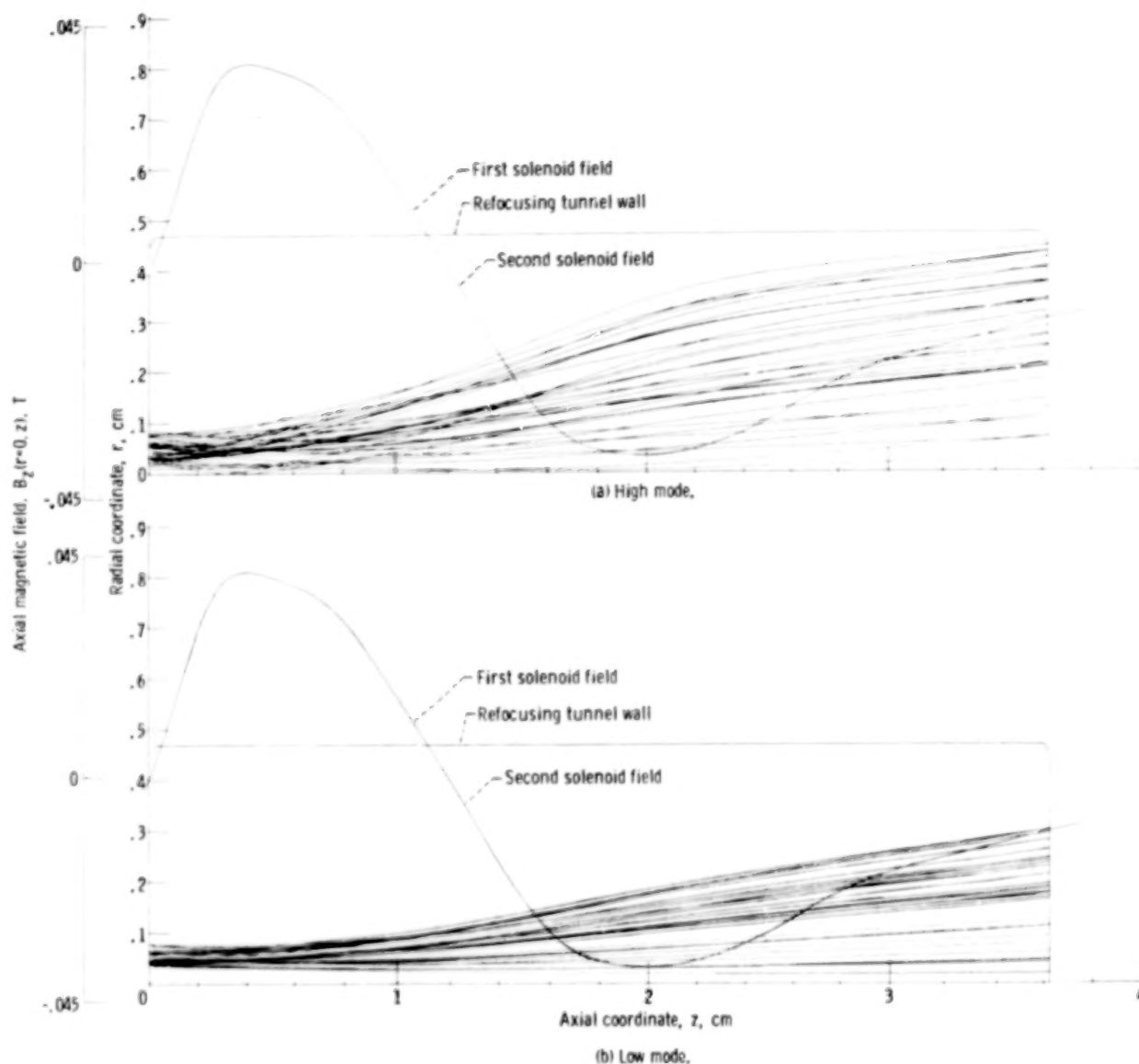


Figure 8. - Charge trajectories and refocusing field profile in the refocusing section for TWT operation over a 10:1 pulse-up in output power.

## MDC Analysis Results and Comparison with Experimental Measurements

### Dual-mode TWT Operation at Saturation

The axisymmetric MDC geometry, the applied potentials, the equipotential lines, and the charge trajectories for the high and low modes are shown in figures 10 and 11, respectively. Analytical and experimental TWT-MDC performances are compared in tables IV and V. The voltages, currents, and powers in these and subsequent tables have been rounded off after computation.

When the predicted and measured currents to the various collector electrodes are compared, it can be seen that the agreement was good for the high mode and poor for the low mode. The differences can be largely explained by subtle differences (less than about 5 to 10 percent in energy) between the computed and actual spent beam energy distributions and by inaccuracies in representing the large number of electrons (each with its own radius and vector velocity) within a given ray by the motion of the ray centroid. Since the difference between the equipotentials in figure 11 is only about 1000 volts, it can be seen that with changes of only a few hundred electron volts of kinetic energy for some of the charges and, in some cases, with only slightly



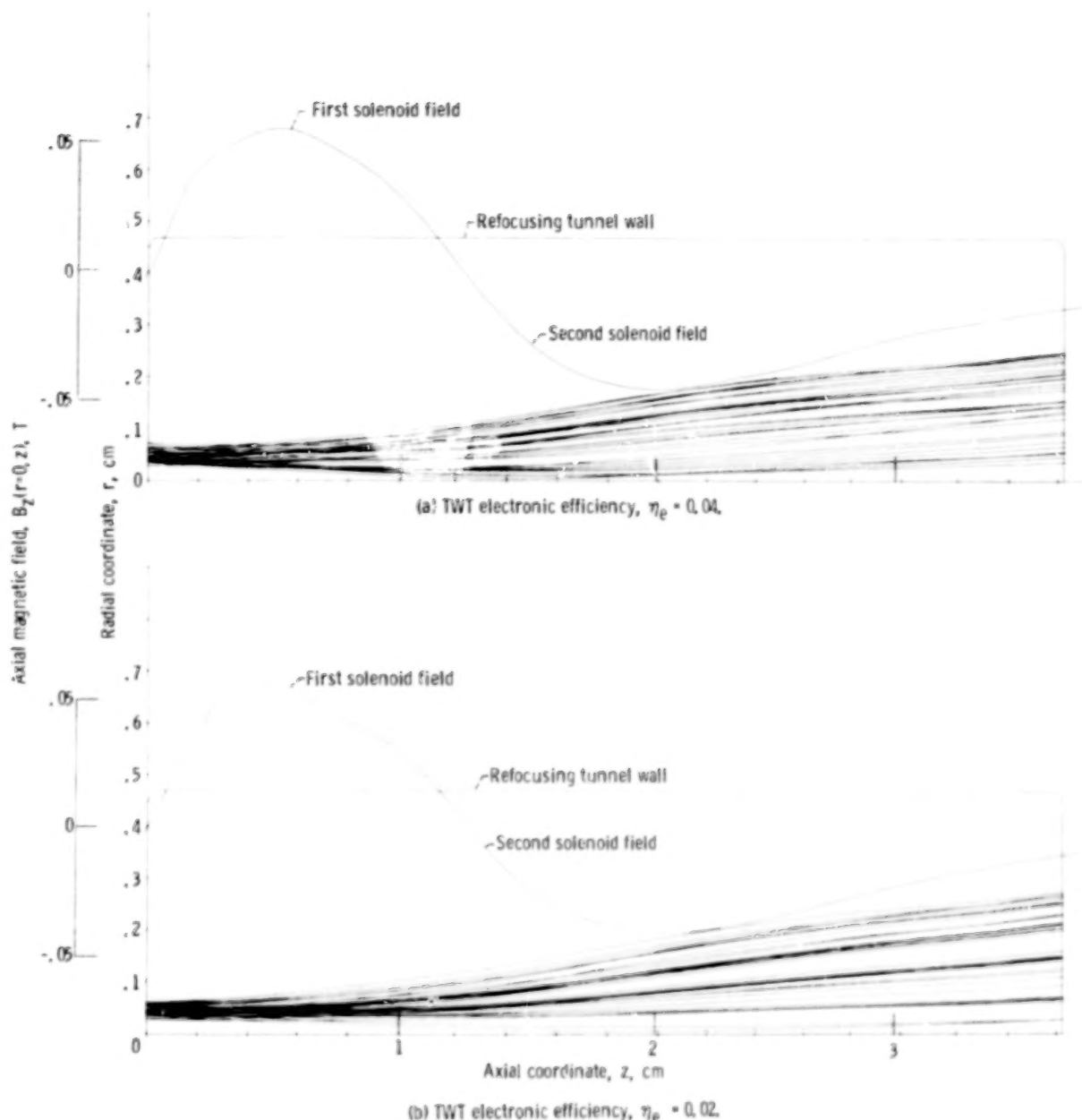


Figure 9. - Charge trajectories and refocusing field profile for TWT operation in linear region.

different injection angles into the MDC, the computed current distribution would more nearly agree with the measured distribution.

The collector efficiencies showed very good agreement. This is of particular importance, since the primary purpose of this analytical design procedure (apart from TWT analysis) is to produce an optimum refocusing system design and a highly efficient MDC geometric design.

Predicting the distribution of current to the electrodes at one particular operating point is considerably less important since the collector and power supplies must be designed to tolerate a wide

range of currents and dissipated powers (see, e.g., ref. 7) to allow for operation under other conditions—in particular, below saturation.

#### Dual-mode TWT Operation Over a 10:1 Pulse-up in Output Power

The MDC geometry, the applied potentials, the equipotential lines, and the charge trajectories for the high and low modes are shown in figures 12 and 13, respectively. Analytical and experimental TWT-MDC performances are compared in tables VI and VII.

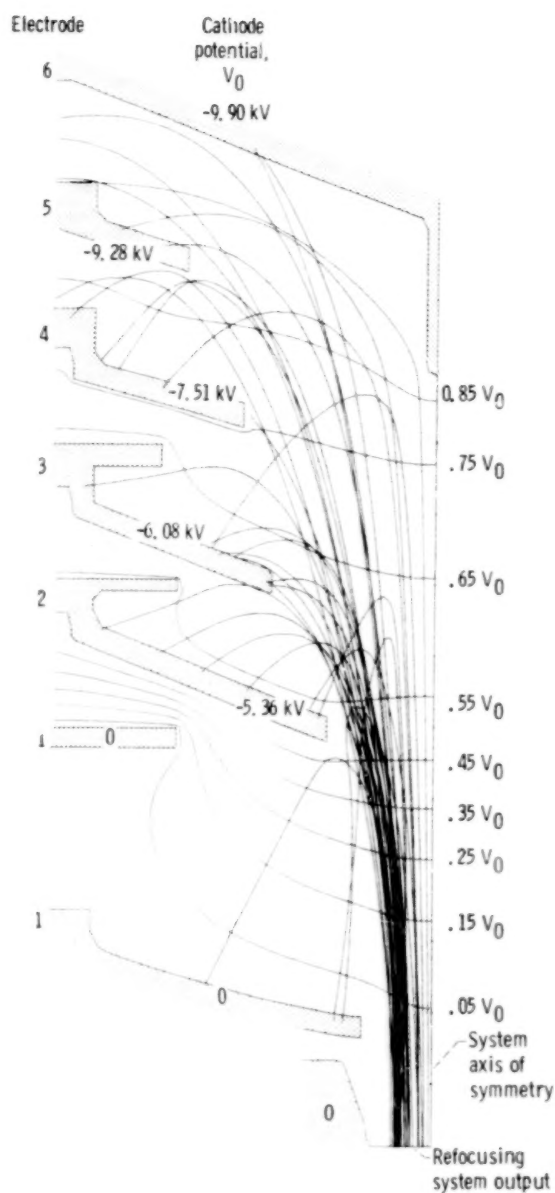


Figure 10. - Charge trajectories in five-stage depressed collector. TWT operating at saturation in high mode (optimized for low mode).

Figures 12 and 13 illustrate what can happen when, at a fixed set of operating conditions, the refocusing system and MDC are required to handle beams which differ radically in character. The refocusing system and MDC were optimized largely for the low (cw) mode and MDC efficiency for the high mode is severely compromised. This can be seen by comparing these results to those for the high mode (fig. 10, table IV) which had identical TWT performance and spent beam but different refocusing system and MDC operating conditions. The resulting reduction in overall efficiency, however, is not

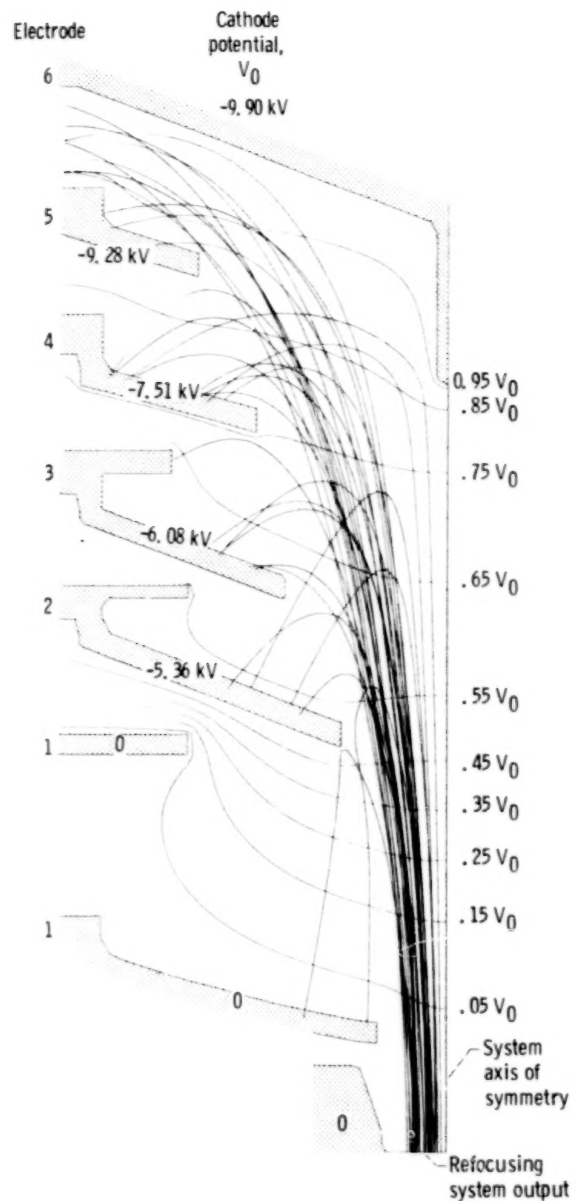


Figure 11. - Charge trajectories in five-stage depressed collector; TWT operating at saturation in low mode (optimized for low mode).

important in certain applications because the high mode represents only very low duty cycle operation.

The computed and measured collector efficiencies showed fair agreement for the high mode and excellent agreement for the low mode.

#### TWT Operation in the Linear Region

The MDC geometry, the applied potentials equipotential lines, and the charge trajectories for TWT operation at electronic efficiencies of 4 and 2 percent are shown in figures 14 and 15, respectively.

TABLE IV. - ANALYTICAL AND EXPERIMENTAL PERFORMANCES OF TELEDYNE MEC TWT MTZ 7000

WITH EXPERIMENTAL FIVE-STAGE DEPRESSED COLLECTOR AND TWT

OPERATING AT SATURATION IN HIGH MODE

[ Computed trajectories shown in fig. 10. ]

## (a) MDC performance

Collecting element	Voltage with respect to ground, kV	Analytical			Experimental		
		Current, mA	Recovered power, W	Kinetic power dissipated, W	Current, mA	Recovered power, W	Kinetic power dissipated, W
TWT body (interception)	0	2	0	12	9	0	80
TWT body (backstreaming)	0	---	0	---	11	0	115
Electrode -							
1 (backstreaming)	0	46	0	247	9	0	52
2	-5.36	101	540	71	95	508	104
3	-6.08	133	807	111	173	1055	175
4	-7.51	85	642	159	79	594	57
5	-9.28	104	962	87	105	975	88
6	-9.90	18	181	40	6	63	32
Collector efficiency, percent		81.4			84.3		

## (b) Final power balance

	Analytical	Experimental
Total rf power conversion (includes circuit and sever losses), W	990	<sup>a</sup> 927
Beam interception losses, W	12	<sup>a</sup> 80
Backstreaming to TWT body, W	0	<sup>b</sup> 115
MDC dissipation (includes backstreaming to electrode 1), W	715	481
Recovered power, W	3132	3195
Total power, W	4849	4798
Direct current power, $I_0 V_0$ , W	4831	4798

<sup>a</sup>Using  $V_0 I_B (1 - \eta_e)$  for the average power of the intercepted electrons.<sup>b</sup>Computed from requirement of final power balance.

TABLE V. - ANALYTICAL AND EXPERIMENTAL PERFORMANCES OF TELEDYNE MEC TWT MTZ 7000

WITH EXPERIMENTAL FIVE-STAGE DEPRESSED COLLECTOR AND TWT

OPERATING AT SATURATION IN LOW MODE

[ Computed trajectories shown in fig. 11.]

## (a) MDC performance

Collecting element	Voltage with respect to ground, kV	Analytical			Experimental		
		Current, mA	Recovered power, W	Kinetic power dissipated, W	Current, mA	Recovered power, W	Kinetic power dissipated, W
TWT body (interception)	0	0	0	0	4	0	39
TWT body (backstreaming)	0	0	0	0	4	0	76
Electrode -							
1 (backstreaming)	0	24	0	135	7	0	48
2	-5.36	49	262	50	62	334	66
3	-6.08	73	446	71	129	783	112
4	-7.51	110	826	141	49	369	38
5	-9.28	134	1247	116	127	1176	89
6	-9.90	0	0	0	8	75	39
Collector efficiency, percent		84.4			85.5		

## (b) Final power balance

	Analytical	Experimental
Total rf power conversion (includes circuit and sever losses), W	589	<sup>a</sup> 617
Beam interception losses, W	0	<sup>a</sup> 39
Backstreaming to TWT body, W	0	<sup>b</sup> 76
MDC dissipation (includes backstreaming to electrode 1), W	513	388
Recovered power, W	2781	2737
Total power, W	3883	3855
Direct current power, $I_0 V_0$ , W	3871	3855

<sup>a</sup>Using  $V_0 I_B (1 - \eta_e)$  for the average power of the intercepted electrons.<sup>b</sup>Computed from requirement of final power balance.

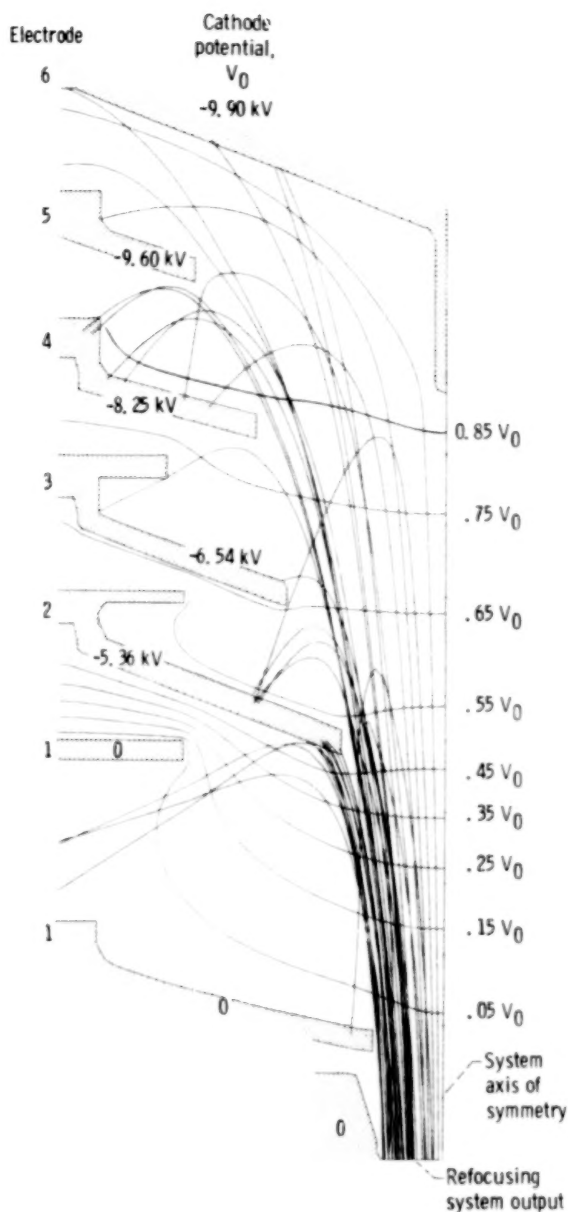


Figure 12. - Charge trajectories in five-stage depressed collector. TWT operating at saturation in high mode (optimized for low mode at  $P_{rf} = 1/10 P_{rf}(\text{high mode})$ ).

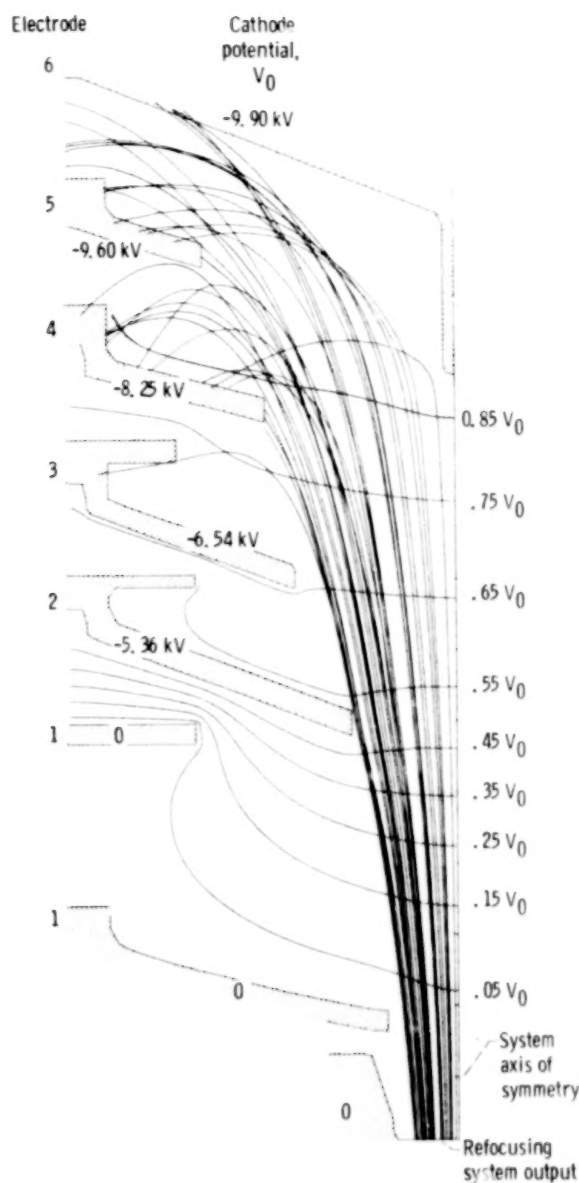


Figure 13. - Charge trajectories in five-stage depressed collector. TWT operating in low mode (optimized for low mode at  $P_{rf} = 1/10 P_{rf}(\text{high mode})$ ).

Analytical and experimental TWT-MDC performances are compared in tables VIII and IX.

Figures 14 and 15 illustrate the potential danger of lens effects in these collectors. One charge, in each case, has insufficient energy (by  $< 1$  percent) to reach electrode 4 and stops in the presence of a convergent lens (see equipotential  $0.95 V_0$  in fig. 15). The resulting backstreaming to the TWT body accounts

for much of the discrepancy between the computed and measured overall efficiencies.

The computed and measured current distributions show relatively poor agreement in both cases. Again, we are dealing with subtle differences between the computed and actual spent beam energy distributions, radii, and injection angles which have a large effect on the electrode current distribution



TABLE VI. - ANALYTICAL AND EXPERIMENTAL PERFORMANCES OF TELEDYNE MEC TWT MTZ 7000  
WITH EXPERIMENTAL FIVE-STAGE DEPRESSED COLLECTOR AND TWT

OPERATING AT SATURATION IN HIGH MODE

[ Computed trajectories shown in fig. 12.]

(a) MDC performance

Collecting element	Voltage with respect to ground, kV	Analytical			Experimental		
		Current, mA	Recovered power, W	Kinetic power dissipated, W	Current, mA	Recovered power, W	Kinetic power dissipated, W
TWT body (interception)	0	2	0	12	9	0	80
TWT body (backstreaming)	0	15	0	83	25	0	202
Electrode -							
1 (backstreaming)	0	110	0	605	38	0	244
2	-5.36	133	712	223	129	693	154
3	-6.54	30	199	30	126	822	145
4	-8.25	92	755	110	71	587	47
5	-9.60	70	674	36	66	632	32
6	-9.90	37	362	52	20	201	36
Collector efficiency, percent		70.4			77.6		

(b) Final power balance

	Analytical	Experimental
Total rf power conversion (includes circuit and sever losses), W	990	<sup>a</sup> 941
Beam interception losses, W	12	<sup>a</sup> 80
Backstreaming to TWT body, W	83	<sup>b</sup> 202
MDC dissipation (includes backstreaming to electrode 1), W	1056	645
Recovered power, W	2702	2935
Total power, W	4843	4803
Direct current power, $I_0 V_0$ , W	4831	4803

<sup>a</sup>Using  $V_0 I_B (1 - \eta_e)$  for the average power of the intercepted electrons.

<sup>b</sup>Computed from requirement of final power balance.

TABLE VII. - ANALYTICAL AND EXPERIMENTAL PERFORMANCE OF TELEDYNE MEC TWT MTZ 7000

WITH EXPERIMENTAL FIVE-STAGE DEPRESSED COLLECTOR AND TWT

OPERATING IN LOW MODE AT  $P_{rf} = \frac{1}{10} P_{rf}$  (HIGH MODE)

[ Computed trajectories shown in fig. 13.]

## (a) MDC performance

Collecting element	Voltage with respect to ground, kV	Analytical			Experimental		
		Current, mA	Recovered power, W	Kinetic power dissipated, W	Current, mA	Recovered power, W	Kinetic power dissipated, W
TWT body (interception)	0	0	0	0	3	0	25
TWT body (backstreaming)	0	0	0	0	2	0	32
Electrode -							
1 (backstreaming)	0	0	0	0	4	0	33
2	-5.36	0	0	0	16	86	39
3	-6.54	27	176	43	25	162	49
4	-8.25	154	1271	169	63	520	17
5	-9.60	181	1737	74	268	2572	98
6	-9.90	29	290	22	16	101	36
Collector efficiency, percent		91.8			91.9		

## (b) Final power balance

	Analytical	Experimental
Total rf power conversion (includes circuit and sever losses), W	89	<sup>a</sup> 91
Beam interception losses, W	0	<sup>a</sup> 25
Backstreaming to TWT body, W	0	<sup>b</sup> 32
MDC dissipation (includes backstreaming to electrode 1), W	309	271
Recovered power, W	3474	3440
Total power, W	3872	3860
Direct current power, $I_0 V_0$ , W	3871	3860

<sup>a</sup>Using  $V_0 I_B (1 - \eta_e)$  for the average power of the intercepted electrons.<sup>b</sup>Computed from requirement of final power balance.

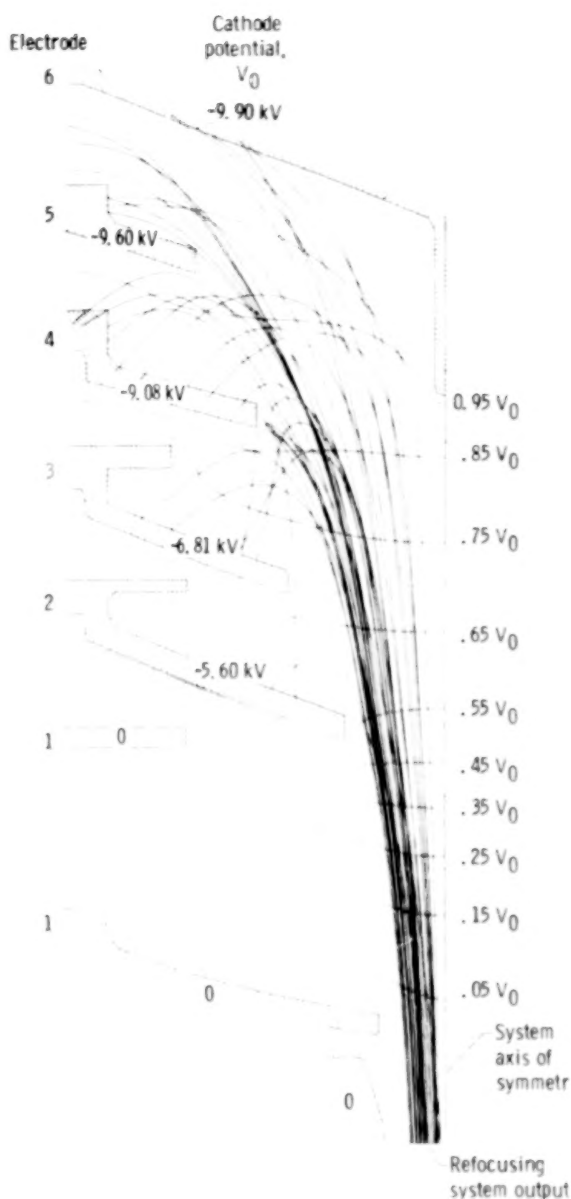


Figure 14. - Charge trajectories in five-stage depressed collector. TWT operating in linear range at  $\eta_e = 0.04$ .

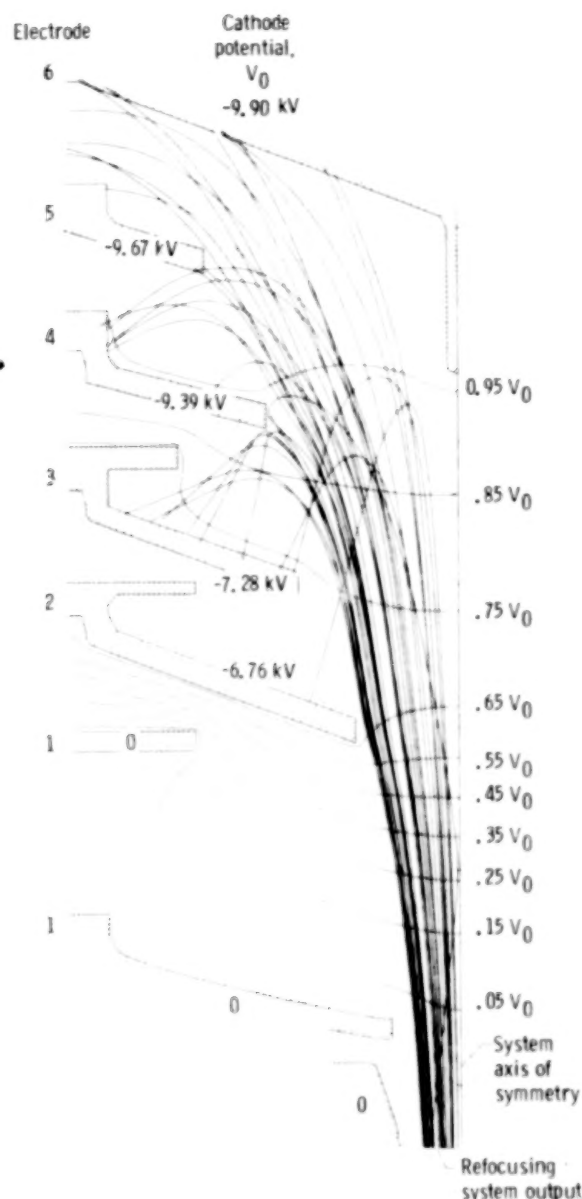


Figure 15. - Charge trajectories in five-stage depressed collector. TWT operating in linear region at  $\eta_e = 0.02$ .

(particularly for a large number of stages to cover a fixed voltage range) but a relatively small effect on collector efficiency.

## Computerized Collector Design

The application of these computing techniques to the design of collectors offers a considerable advance in MDC technology. The extension of these techniques from data analysis to MDC design rests on the ability to accurately compute a mathematical

model of the spent beam. The ability to design an MDC with a predictable performance is a measure of the accuracy with which the spent beam can be predicted.

The collector discussed thus far was developed by a time-consuming empirical process. Although it does provide excellent efficiency (with a diameter of 5.1 cm, a length of 7.6 cm, and five depressed stages), it is larger, heavier, and more complex than desired. Figure 16 shows a four-stage MDC with a diameter of 2.4 centimeters and a length of 4.3 centimeters which was designed with a computer and predicted to

TABLE VIII. - ANALYTICAL AND EXPERIMENTAL PERFORMANCES OF TELEDYNE MFC TWT MTZ 7000  
WITH EXPERIMENTAL FIVE-STAGE DEPRESSED COLLECTOR AND TWT  
OPERATING IN LINEAR RANGE AT  $\eta_c = 0.04$

[ Computed trajectories shown in fig. 14. ]

(a) IDC performance

Collecting element	Voltage with respect to ground, kV	Analytical			Experimental		
		Current, mA	Recovered power, W	Kinetic power dissipated, W	Current mA	Recovered power, W	Kinetic power dissipated, W
TWT body (interception)	0	0	0	0	3	0	26
TWT body (backstreaming)	0	12	0	110	5	0	48
Electrode -							
1 (backstreaming)	0	0	0	0	8	0	51
2	-5.60	24	137	49	33	187	40
3	-6.81	66	449	124	37	254	65
4	-9.08	122	1109	57	87	789	26
5	-9.60	122	1173	48	198	1903	84
6	-9.90	44	436	32	19	190	40
Collector efficiency, percent		88.7			90.4		

(b) Final power balance

	Analytical	Experimental
Total rf power conversion (includes circuit and sever losses), W	159	<sup>a</sup> 158
Beam interception losses, W	0	<sup>a</sup> 26
Backstreaming to TWT body, W	110	<sup>b</sup> 48
MDC dissipation (includes backstreaming to electrode 1), W	310	306
Recovered power, W	3304	3323
Total power, W	3883	3860
Direct current power, $I_0 V_0$ , W	3871	3860

<sup>a</sup>Using  $V_0 I_B (1 - \eta_c)$  for the average power of the intercepted electrons.

<sup>b</sup>Computed from requirement of final power balance.

TABLE IX. - ANALYTICAL AND EXPERIMENTAL PERFORMANCES OF TELEDYNE MEC TWT MTZ 7000

WITH EXPERIMENTAL FIVE-STAGE DEPRESSED COLLECTOR AND TWT

OPERATING IN LINEAR RANGE AT  $\eta_e = 0.02$ 

[ Computed trajectories shown in fig. 15.]

(a) MDC performance

Collecting element	Voltage with respect to ground. kV	Analytical			Experimental		
		Current, mA	Recovered power, W	Kinetic power dissipated W	Current, mA	Recovered power, W	Kinetic power dissipated, W
TWT body (interception)	0	0	0	0	3	0	25
TWT body (backstreaming)	0	12	0	115	4	0	51
Electrode -							
1 (backstreaming)	0	0	0	0	4	0	34
2	-6.76	12	82	30	12	84	19
3	-7.28	103	746	181	46	334	63
4	-9.39	100	941	31	131	1232	23
5	-9.67	120	1158	38	177	1708	60
6	-9.90	44	436	30	13	130	21
Collector efficiency, percent		88.8			92.8		

(b) Final power balance

	Analytical	Experimental
Total rf power conversion (includes circuit and sever losses), W	75	<sup>a</sup> 75
Beam interception losses, W	0	<sup>a</sup> 25
Backstreaming to TWT body, W	115	<sup>b</sup> 51
MDC dissipation (includes backstreaming to electrode 1), W	310	221
Recovered power, W	3363	3488
Total power, W	3863	3860
Direct current power, $I_0 V_0$ , W	3871	3860

<sup>a</sup>Using  $V_0 I_B (1 - \eta_e)$  for the average power of the intercepted electrons.<sup>b</sup>Computed from requirement of final power balance.



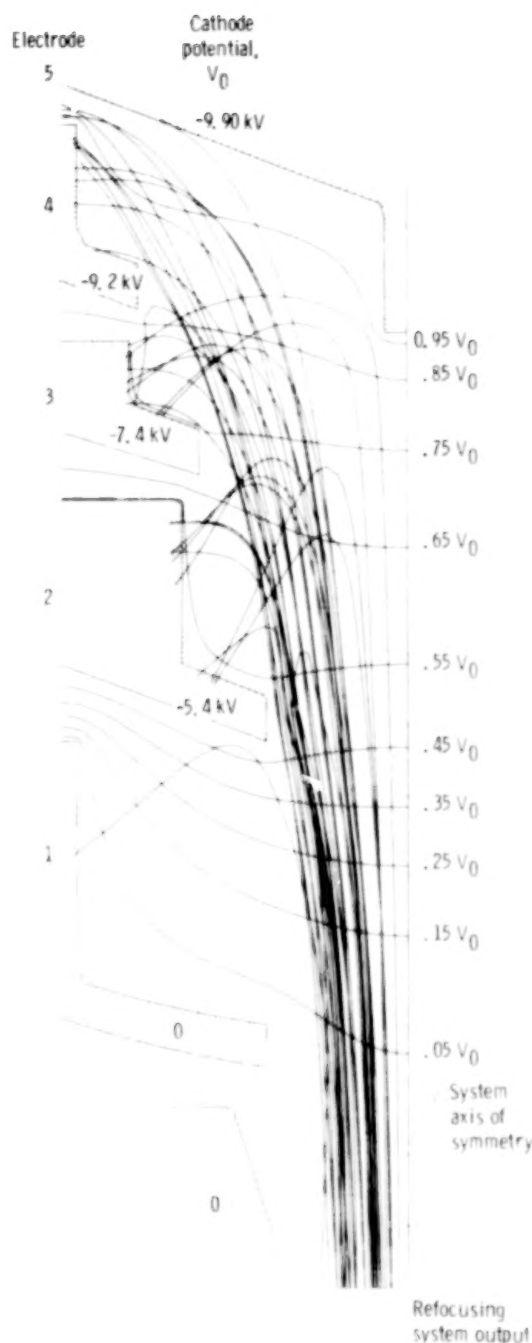


Figure 16. - Charge trajectories in four-stage, 2.4-centimeter-diameter depressed collector. TWT operating at saturation in low mode.

have an efficiency of 83.8 percent for the low mode at saturation.

This collector was subsequently built and tested. The results are shown in table X. The computed and measured electrode current distributions show reasonable agreement in some cases; the major discrepancy is the distribution of current between

electrodes 2 and 3. The collector efficiencies show very good agreement.

When experimentally optimized, this collector produced an efficiency of 83.0 percent. This required a relatively small adjustment of the refocusing field profile and adjustments of the MDC voltages in the range 2.2 to 7.4 percent of nominal values (ref. 7). Such optimizations can be performed quickly and easily since they involve changes exterior to the TWT-MDC vacuum envelope.

## Concluding Remarks

A computational design technique for the TWT-MDC system was described. TWT and MDC performances were analytically and experimentally evaluated at a number of distinct operating points of an octave-bandwidth dual-mode TWT. The operating points were chosen to cover a wide range of TWT applications, from dual-mode operation at saturation to operation in the linear, low-distortion range.

In general, very good agreement was obtained between the computed and measured collector efficiencies. The agreement between computed and measured current distributions was good in some cases but poor in others. The electrode current distribution is much more sensitive to small changes in the distributions of spent beam energy, injection angle, and radius than is the collector efficiency. Additional studies on more TWT samples (where accurate TWT parameters are available) and additional refinement of analytic tools are required to further improve the accuracy of the computations—in particular, in regards to the electrode current distribution.

The computer design of an efficient MDC was demonstrated with a highly efficient, 2.4-centimeter-diameter, four-stage collector that could replace the 5.1-centimeter-diameter, five-stage collector originally tested.

The analytical tools used appear to be sufficiently refined to design efficient collectors for this class of TWT. For maximum efficiency, some experimental optimization (e.g., collector voltages and aperture sizes) will most likely be required. For TWT's of higher perveance and electronic efficiency, additional verification of the design process is needed.

Lewis Research Center  
National Aeronautics and Space Administration  
Cleveland, Ohio, January 7, 1981

TABLE X. - ANALYTICAL AND EXPERIMENTAL PERFORMANCES OF TELEDYNE MEC TWT MTZ 7000  
WITH 2.4-CENTIMETER-DIAMETER FOUR-STAGE DEPRESSED COLLECTOR AND TWT  
OPERATING AT SATURATION IN LOW MODE

[ Computed trajectories shown in fig. 16.]

(a) MDC performance

Collecting element	Voltage with respect to ground, kV	Analytical			Experimental		
		Current mA	Recovered power, W	Kinetic power dissipated, W	Current mA	Recovered power, W	Kinetic power dissipated, W
TWT body (interception)	0	0	0	0	4	0	38
TWT body (backstreaming)	0	12	0	68	16	0	89
Electrode -							
1 (backstreaming)	0	12	0	66	7	0	44
2	-5.40	110	594	141	181	979	220
3	-7.40	110	814	136	54	398	85
4	-9.20	139	1282	117	127	1171	112
5	-9.90	7	72	7	7	73	37
Collector efficiency, percent		83.8			81.7		

(b) Final power balance

	Analytical	Experimental
Total rf power conversion (includes circuit and sever losses), W	589	<sup>a</sup> 615
Beam interception losses, W	0	<sup>a</sup> 38
Backstreaming to TWT body, W	68	<sup>b</sup> 89
MDC dissipation (includes backstreaming to electrode 1), W	467	498
Recovered power, W	2762	2621
Total power, W	3886	3861
Direct current power, $I_0 V_0$ , W	3871	3861

<sup>a</sup>Using  $V_0 I_B (1 - \eta_e)$  for the average power of the intercepted electrons.

<sup>b</sup>Computed from requirement of final power balance.

## Appendix—Symbols<sup>a</sup>

$B_z$	axial magnetic field, T	$P_{body}$	(total rf losses in TWT) + (true beam interception losses)
$e$	electronic charge	$P_{coll}$	total power in spent beam that enters MDC
$I_B$	true interception current in forward direction	$P_{rf}$	total rf output
$I_{body}$	$I_B + I_S$	$\bar{V}$	average potential of intercepted electrons
$I_{en}$	collector current to $n^{\text{th}}$ electrode	$V_0$	cathode potential (always negative for work reported herein)
$I_{e1}$	backstreaming current to undepressed collector electrode	$\eta_e$	TWT electronic efficiency, $(P_{rf} + \text{Circuit losses})/I_0 V_0$
$I_0$	cathode current or beam current		
$I_S$	backstreaming current to TWT body		

## References

1. Kosmahl, H. G.: A Novel, Axisymmetric, Electrostatic Collector for Linear Beam Microwave Tubes. NASA TN D-6093, 1971.
2. Kosmahl, H. G.; and Ramins, P.: Small-Size 81- to 83.5-Percent Efficient 2- and 4-Stage Depressed Collectors for Octave-Bandwidth High-Performance TWT's. IEEE Trans. Electron Devices, vol. ED-24, no. 1, Jan. 1977, pp. 36-44.
3. Kosmahl, H. G.: An Electron Beam Collector. U.S. Patent No. 3,764,850, Oct. 1973.
4. Stankiewicz, N.: Analysis of Spent Beam Refocusing to Achieve Optimum Collector Efficiency. IEEE Trans. Electron Devices, vol. ED-24, no. 1, Jan. 1977, pp. 32-26.
5. Dayton, J. A., Jr.; et al.: Analytical Prediction with Multidimensional Computer Programs and Experimental Verification of the Performance, at a Variety of Operating Conditions, of Two Traveling Wave Tubes with Depressed Collectors. NASA TP-1449, 1979.
6. Dayton, J. A., Jr.; et al.: Analytical Prediction and Experimental Verification of TWT and Depressed Collector Performance Using Multidimension Computer Programs. IEEE Trans. Electron Devices, vol. ED-26, no. 10, Oct. 1979, pp. 1589-1597.
7. Ramins, Peter; and Fox, Thomas A.: Performance of Computer-Designed Small-Sized Four Stage Depressed Collector for Operation of Dual-Mode Traveling Wave Tube at Saturation. NASA TP-1832, 1981.
8. Herrmannsfeldt, W. B.: Electron Trajectory Program. SLAC-166, Stanford Linear Accelerator Center, 1973.
9. Ramins, P.; and Fox, T. A.: Multistage Depressed Collector with Efficiency of 90 to 94 Percent for Operation of a Dual-Mode Traveling Wave Tube in the Linear Region. NASA TP-1670, 1980.
10. Vaughan, J. R. M.: Representation of Axisymmetric Magnetic Fields in Computer Programs. IEEE Trans. Electron Devices, vol. ED-19, no. 2, Feb. 1972, pp. 144-151.
11. Stankiewicz, N.: A Matrix Solution for the Simulation of Magnetic Fields with Ideal Current Loops. IEEE Trans. Electron Devices, vol. ED-26, no. 10, Oct. 1979, pp. 1598-1601.
12. Kosmahl, Henry G.: How to Quickly Predict the Overall TWT and the Multistage Depressed Collector Efficiency. IEEE Trans. Electron Devices, vol. ED-27, no. 3, Mar. 1980, pp. 526-529.

1. Report No. <b>NASA TP-1831</b>	2. Government Accession No.	3. Recipient's Catalog No.	
4. Title and Subtitle <b>ANALYTICAL PREDICTION AND EXPERIMENTAL VERIFICATION OF PERFORMANCE, AT VARIOUS OPERATING CONDITIONS, OF A DUAL-MODE TRAVELING WAVE TUBE WITH MULTISTAGE DEPRESSED COLLECTORS</b>		5. Report Date July 1981	
		6. Performing Organization Code <b>506-61-32</b>	
7. Author(s) <b>James A. Dayton, Jr., Henry G. Kosmahl, Peter Ramins, and Norbert Stankiewicz</b>		8. Performing Organization Report No. <b>E-577</b>	
		10. Work Unit No.	
9. Performing Organization Name and Address <b>National Aeronautics and Space Administration Lewis Research Center Cleveland, Ohio 44135</b>		11. Contract or Grant No.	
		13. Type of Report and Period Covered <b>Technical Paper</b>	
12. Sponsoring Agency Name and Address <b>National Aeronautics and Space Administration Washington, D. C. 20546</b>		14. Sponsoring Agency Code	
15. Supplementary Notes			
16. Abstract  A comparison of analytical and experimental results is presented for a high performance dual-mode traveling wave tube operated over a wide range of conditions. The computations are carried out with advanced multidimensional computer programs. These programs model the electron beam as a series of disks or rings of charge and follow their trajectories from the rf input of the TWT through the slow-wave structure and the refocusing system to their points of impact in the depressed collector. TWT performance, collector efficiency, and collector current distribution are computed and compared with measurements. Very good agreement was obtained between computed and measured TWT performance and collector efficiencies, and the computer design of a highly efficient collector was demonstrated.			
17. Key Words (Suggested by Author(s)) <b>Traveling wave tube Multistage depressed collector Spent beam refocusing</b>		18. Distribution Statement <b>Unclassified - unlimited STAR Category 33</b>	
19. Security Classif. (of this report) <b>Unclassified</b>	20. Security Classif. (of this page) <b>Unclassified</b>	21. No. of Pages <b>26</b>	22. Price* <b>A04</b>



90%

END

10-16-81